

# Evaluation of human thorax FE model in various impact scenarios

M. Jansová<sup>a,\*</sup>, L. Hynčák<sup>a</sup>, H. Čechová<sup>a</sup>, J. Toczyski<sup>b</sup>,  
D. Gierczycka-Zbrozek<sup>b</sup>, P. Baudrit<sup>c</sup>

<sup>a</sup>*New Technologies – Research Centre, University of West Bohemia, Univerzitní 8, 306 14 Plzeň, Czech Republic*

<sup>b</sup>*Institute of Aeronautics and Applied Mechanics, Warsaw University of Technology, ul. Nowowiejska 29, 00-665 Warsaw, Poland*

<sup>c</sup>*CEESAR – European Centre of Studies on Safety and Risk Analysis, 132, Rue des Suisses, 92000, Nanterre, France*

Received 17 March 2015; received in revised form 19 June 2015

---

## Abstract

The study focused on the validation of the 50<sup>th</sup> percentile male model — a detailed FE model of the thoracic segment of the human body developed within project *Development of a Finite Element Model of the Human Thorax and Upper Extremities* (THOMO) co-funded by the European Commission (7<sup>th</sup> Framework Programme). The model response was tested in three impact scenarios: frontal, lateral and oblique. The resulting impactor contact force vs. time and chest deflection vs. time responses were compared with experimental results. The strain profile of the 5th rib was checked with lateral and oblique strain profiles from post-mortem human subject (PMHS) experiments. The influence of heart and lungs on the mechanical response of the model was assessed and the material data configuration, giving the most biofidelic thorax behaviour, was identified.

© 2015 University of West Bohemia. All rights reserved.

*Keywords:* human body, thorax, validation, impact, finite element model

---

## 1. Introduction

In the last decade, the legalisation of computer simulated crash tests with virtual human body models is one of the goals of automotive industry [5]. This testing requires a biofidelic model of the human body. There is a wide range of existing virtual human body models with various level of accuracy — ranging from simplified multibody models, allowing relatively fast simulations and approximated injury prediction, up to models respecting anatomical details that serve for detailed analysis of injury assessment under impact loading. Some models even allow scaling to different anthropometry.

Detailed review of development of biomechanical numerical models of the human body was performed by Yang [20]. The Human Model for Safety (HUMOS) programme running from 1997 to 2001 was the first step toward the development of commonly accepted models and computer methods [13]. It was followed by the HUMOS2 project from 2001 to 2006 [17].

One of the more detailed full human body models is the Total Human Model for Safety (THUMS<sup>TM</sup>) developed by Toyota Motor Corporation and Toyota Central R&D Labs to predict internal organ injury [6, 16].

Currently the Global Human Body Model Consortium (GHBMC) — an international consortium of nine automakers and two suppliers working with research institutes and government agencies creates the world's most detailed midsize (50<sup>th</sup> percentile) male human body model [3].

---

\*Corresponding author. Tel.: +420 377 634 710, e-mail: jansovam@ntc.zcu.cz.

The paper describes the validation process of the thorax model developed within the THOMO project in cooperation with GHBM. The goal of THOMO project was the development of numerical models, focusing on the validation of rib strain fields, in order to exhibit the rib fracture mechanisms.

## 2. Methodology

### 2.1. Reference model

In order to facilitate the thorax model development, the complete GHBM model (mid-size male) was simplified by the Thorax Center of Expertise at the University of Virginia and forwarded to the THOMO consortium members for refinement. Material properties of particular tissues were provided by Centers of Expertise (COE). The ribs were defined as breakable with a threshold of plastic failure strain of 1.8 %.

Further development of the model focused on resolving geometrical and numerical instabilities, re-meshing, updating the musculature and expanding the range of available body positions of the model. Initial configuration (seated with upper arms aligned with the thorax) was modified in order to obtain a model with lifted arms, necessary for lateral and oblique pendulum impact setups (Fig. 1). The PMHS tests, carried out within the THOMO project were performed with arms lifted [10].

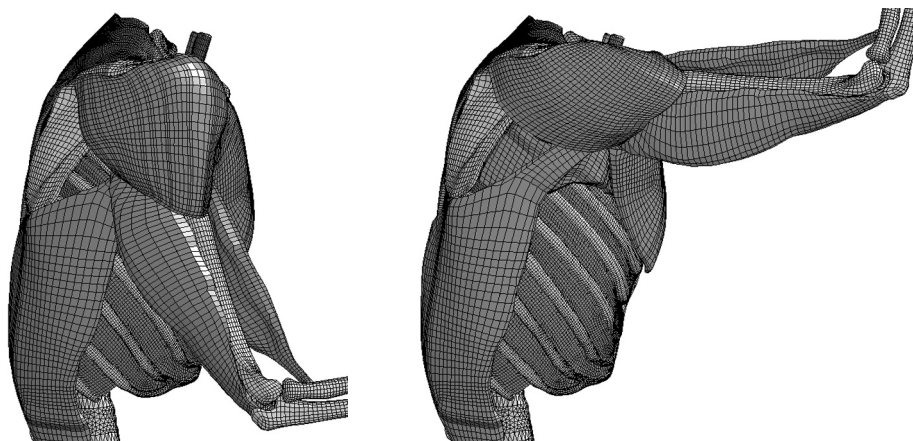


Fig. 1. Detail of the muscles of right upper arm of the THOMO model for frontal impact (left) and lateral and oblique impact (right)

### 2.2. Validation tests

The extensive review of available validation test data was performed within the THOMO project. These data are in the form of validation corridors formed by the response of cadavers to given test setup. Based on the review results, suitable tests were chosen in cooperation with the Thorax Center of Expertise at the University of Virginia. The THOMO thorax model was validated in three validation scenarios, namely frontal impact, lateral impact and oblique impact, using the pendulum impactor setup.

The impact test scenarios have been prepared in LS-Dyna software. According to the experimental test setups, the occupant model was seated on a rigid plate and a sliding contact was defined between the plate, pelvis and lower extremities. The rigid plate was fixed at all degrees of freedom (DOF). The occupant model had a full range of motion at all DOF. The impactor

was modelled as a rigid body with initial velocity that corresponded to a reference experimental test. The impactor had only one DOF in direction of the impact for frontal and lateral tests. For the oblique test it had two DOF in the transverse plane at the level of impact direction. The influence of gravity was not considered in the study.

The strain profiles of the 5<sup>th</sup> rib were drawn for the lateral and oblique setups. The strain distribution was plotted as a function of the curvilinear abscissa with costo-transverse joint at  $s = 0\%$  and costo-chondral joint at  $s = 100\%$  (Fig. 2). These strain profiles can be used as a tool for rib fracture prediction [10].

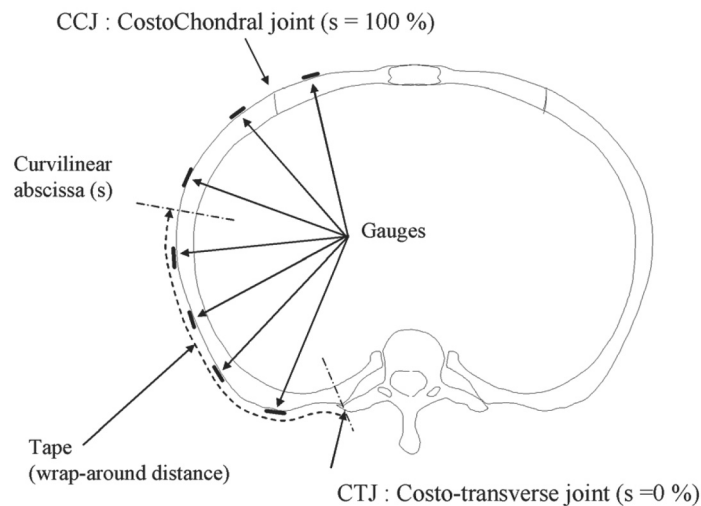


Fig. 2. Definition of the curvilinear abscissa for rib strain profile [10]

Initial series of simulations was performed using the reference model, and then a parametric study was performed. The range of changes covered material properties of internal organs, rib and sternum in order to obtain more biofidelic response in the validation scenarios. The lungs are represented by 10 639 solid elements and the heart by 3 380 solid elements (Fig. 3, left). The ribcage has significantly higher number of solid elements — 49 000 for ribs, 10 400 for costal cartilage and 1 720 for sternum (Fig. 3, right).

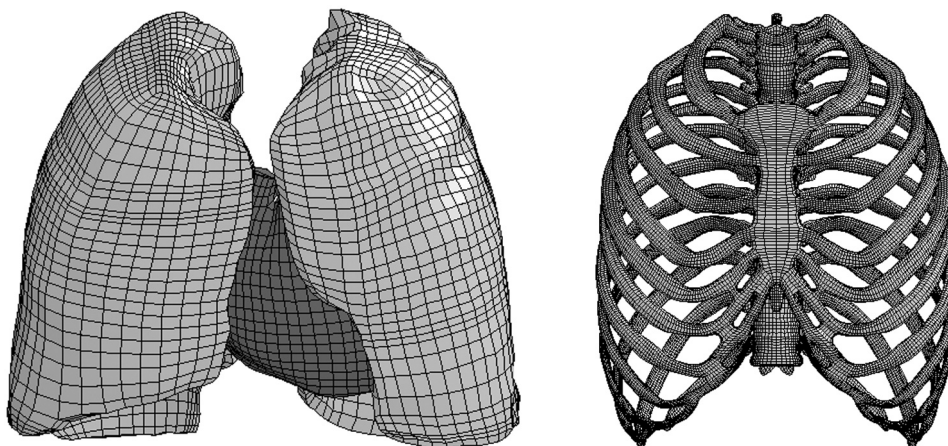


Fig. 3. FE model of heart and lungs (left) and ribcage (right)

### Frontal impact

For the frontal impact (according to Kroell [8,9]), the impactor with mass of 23.4 kg and outer diameter of 152.4 mm was used at two energy levels, defined by the impact velocity of 4.3 m/s and 6.7 m/s. The impactor was aligned with the sternum centreline, at the level of 4<sup>th</sup> sternocostal joint (Fig. 4, left). The reference test responses, external thorax deflection and impactor contact force were monitored.

### Oblique impact

For the oblique impact, a test scenario developed at the Ohio State University (OSU) was used as a reference [15]. The impactor of mass of 23.97 kg and outer diameter of 152.4 mm was centred on the middle point of the 6<sup>th</sup> rib and rotated by 30° of pure lateral, Fig. 4, middle. The impact velocity was 2.5 m/s. The impactor contact force, thorax deflection and strain along the ribs were monitored.

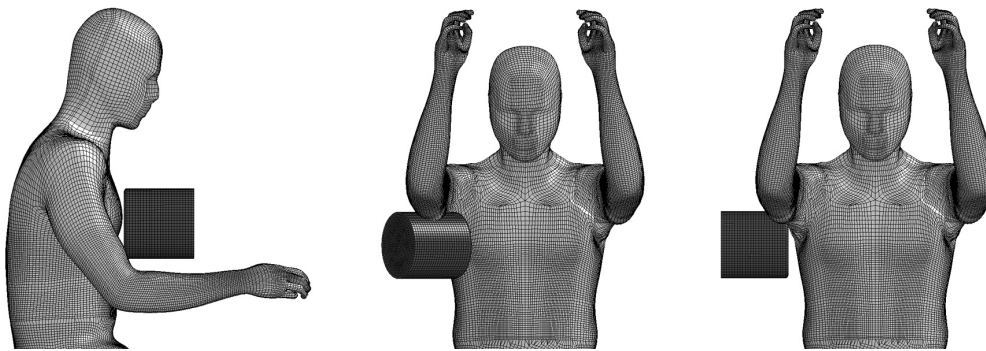


Fig. 4. Test setup of the frontal (left), oblique (middle) and lateral (right) impact

### Lateral impact

In the lateral impact scenarios the impactor was rotated 90 degrees with respect to the initial frontal position and aligned with the half-distance between the model sternum and back measured in the sagittal plane at two different heights. One of the setups was based on the Ohio State University (OSU) configuration with the impactor at the level of 6<sup>th</sup> rib [15] — the impactor mass of 23.97 kg, outer diameter of 152.4 mm and the impact velocity was 2.5 m/s. Second setup based on HSRI (*Highway Safety Research Institute*) test scenario [12] with impactor at the level of the 4<sup>th</sup> sternocostal joint. The impactor had a mass of 23.4 kg and outer diameter of 152.4 mm. The impact velocity was 4.3 m/s. The difference in impactor position is 9 mm, therefore only OSU lateral setup is shown in Fig. 4, right. The impactor contact force and strain along the ribs were the monitored outputs.

### 2.3. Material models for heart and lungs

The THOMO thorax model is too stiff in the frontal impact in comparison to validation corridors. Therefore an alteration of heart and lungs material models is considered as one modification of the THOMO thorax model. The influence of material parameters for heart and lungs has been presented in [4]. The study used various levels of simplification of the THOMO thorax model and has shown that the heart and lungs behaviour was not physical and some material definitions caused numerical instability of the model. A similar parametric study of the material properties was performed in current study. The material properties used for the analysis are listed in Table 1

Table 1. Material models and parameters of heart materials

	Parameters	Material type and id in LS-Dyna	Reference
Reference material	Mass density: $\rho = 1\,000\text{ kg/m}^3$ , Diastolic material coefficients: $C = 1.085\text{ kPa}$ , $B_1 = 24.26$ , $B_2 = 40.52$ , $B_3 = 1.63$ , Pressure in the muscle tissue: $P = 2.482\,5\text{ GPa}$	Hyperelastic MAT_128	[2]
Material 1	Mass density: $\rho = 1\,000\text{ kg/m}^3$ Bulk modulus: $K = 1.33\text{ MPa}$ Short-time shear modulus: $G_0 = 0.22\text{ MPa}$ Long-time shear modulus: $G_{\text{inf}} = 0.075\text{ MPa}$ Decay constant: $\beta = 1\text{ 1/ms}$	Viscoelastic MAT_006	[7]
Material 2	Nominal strain [%] vs. Nominal stress [kPa] 10 5.4 20 12.4 30 28.0 50 374.9	Low density foam MAT_057	[6]
Material 3	Mass density: $\rho = 1\,000\text{ kg/m}^3$ Bulk modulus: $K = 0.066\text{ MPa}$ Short-time shear modulus: $G_0 = 0.014\text{ MPa}$ Long-time shear modulus: $G_{\text{inf}} = 0.010\,7\text{ MPa}$ Decay constant: $\beta = 1\text{ 1/ms}$	Viscoelastic MAT_006	[11]
Material 4	Mass density: $\rho = 1\,000\text{ kg/m}^3$ Bulk modulus: $K = 2.6\text{ MPa}$ Short-time shear modulus: $G_0 = 0.44\text{ MPa}$ Long-time shear modulus: $G_{\text{inf}} = 0.15\text{ MPa}$ Decay constant: $\beta = 0.25\text{ 1/ms}$	Viscoelastic MAT_006	[14] quoting [18, 19]
Material 5	Data from THOMO consortium partners		

(heart) and Table 2 (lungs). Because heart and lungs in the model show hourglassing effect, the influence of two types of hourglass control (parameter IHQ) was tested as well by changing the stiffness form of type 2 Flanagan-Belytschko (IHQ = 4) to Flanagan-Belytschko with exact volume integration (IHQ = 3).

#### 2.4. Material models for ribs and sternum

Assuming that the mechanical response of the thorax is affected significantly by the ribcage stiffness [1], the influence of ribs and sternum material parameters on the model behaviour was studied as well. The ribs and the sternum cortical bone in the reference model were modelled by an elasto-plastic rate dependent material with parameters listed in Table 3. The lowest value of Young’s modulus for the rib cortical bone found in the literature was 2.32 GPa [21]. This value was used for the “altered ribs” model, while other material parameters were kept same as for the reference model. For sternum, parameters of an elastic material with density of 1 800 kg/m<sup>3</sup> and Young’s modulus of 2.5 GPa were found in [11]. Therefore in the “altered sternum” model these parameters were used with an elastic definition for the sternum material.

Table 2. Material models and parameters of lungs materials

	Parameters	Material type and id in LS-Dyna	Reference
Reference material	Mass density: $\rho = 288 \text{ kg/m}^3$ , Bulk modulus: $K = 2.66 \text{ MPa}$ , Material coefficients: $\Delta = 0.1 \text{ mm}$ , $C = 1.115\text{e-}3 \text{ MPa}$ , $\alpha = 0.213$ , $\beta = -0.343$ , $C_1 = 1.002\text{e-}3 \text{ MPa}$ , $C_2 = 2.04$	Transversely anisotropic MAT_129	[22]
Material 1	Mass density: $\rho = 600 \text{ kg/m}^3$ Young's modulus: $E = 0.01 \text{ MPa}$	Low density foam MAT_057	[7] quoting [18]
Material 2	Nominal strain [%] vs. Nominal stress [kPa] 10 7.9 20 14.1 30 20.1 50 31.7	Low density foam MAT_057	[6]
Material 3	Mass density: $\rho = 1000 \text{ kg/m}^3$ Bulk modulus: $K = 0.066 \text{ MPa}$ Short-time shear modulus: $G_0 = 0.014 \text{ MPa}$ Long-time shear modulus: $G_{\text{inf}} = 0.0107 \text{ MPa}$ Decay constant: $\beta = 1 \text{ 1/ms}$	Viscoelastic MAT_006	[11]
Material 4	Mass density: $\rho = 1000 \text{ kg/m}^3$ (taken from Mat3) Bulk modulus: $K = 0.066 \text{ MPa}$ (taken from Mat3) Short-time shear modulus: $G_0 = 22.4 \text{ kPa}$ Long-time shear modulus: $G_{\text{inf}} = 7.5 \text{ kPa}$ Decay constant: $\beta = 0.25 \text{ 1/ms}$	Viscoelastic MAT_006	[14]
Material 5	Mass density: $\rho = 600 \text{ kg/m}^3$ Bulk modulus: $K = 0.22 \text{ MPa}$ Short-time shear modulus: $G_0 = 0.02 \text{ MPa}$ Long-time shear modulus: $G_{\text{inf}} = 0.075 \text{ MPa}$ Decay constant: $\beta = 1 \text{ 1/ms}$ (based on other publications)	Viscoelastic MAT_006	[14] quoting [18, 19]
Material 6	Mass density: $\rho = 600 \text{ kg/m}^3$ Bulk modulus: $K = 0.22 \text{ MPa}$ Short-time shear modulus: $G_0 = 0.02 \text{ MPa}$ Long-time shear modulus: $G_{\text{inf}} = 0.075 \text{ MPa}$ Decay constant: $\beta = 0.25 \text{ 1/ms}$	Viscoelastic MAT_006	[14] quoting [18, 19]
Material 7	Mass density: $\rho = 600 \text{ kg/m}^3$ (taken from Mat5) Bulk modulus: $K = 0.22 \text{ MPa}$ (taken from Mat5) Short-time shear modulus: $G_0 = 22.4 \text{ kPa}$ Long-time shear modulus: $G_{\text{inf}} = 7.5 \text{ kPa}$ Decay constant: $\beta = 0.25 \text{ 1/ms}$	Viscoelastic MAT_006	[14]

Table 3. Material parameters of rib and sternum cortical bone

	Mass density $\rho$ [kg/m <sup>3</sup> ]	Young's modulus $E$ [GPa]	Poisson's ratio	Yield stress [GPa]	Tangent modulus [GPa]	Reference
Reference material (ribs and sternum)	2 000	10.18	0.3	0.065 3	2.3	[23]
Altered ribs	2 000	2.32	0.3	0.065 3	2.3	[21]
Altered sternum	1 800	2.5	0.3	–	–	[11]

### 3. Results

#### 3.1. Mechanical response

The validation tests presented in paragraph 2.2 were performed with reference material parameters for heart (Table 1), lungs (Table 2) and rib and sternum (Table 3).

##### Frontal impact — high speed (6.7 m/s)

The contact impactor force results of the frontal test are shown in Fig. 5, left. The force was slightly lower than the corridor in the initial phase, the first peak agreed well with the corridor but was delayed in time, and the second peak exceeded the upper corridor boundary. The resulting thorax deflection (Fig. 5, right) fit the corridor until 13ms and then decreased at a higher rate than the experimental reference. The contact impactor force versus thorax deflection results are shown in Fig. 6. Only the initial part fit the corridor. The occupant model thorax was stiffer compared to the experimental test.

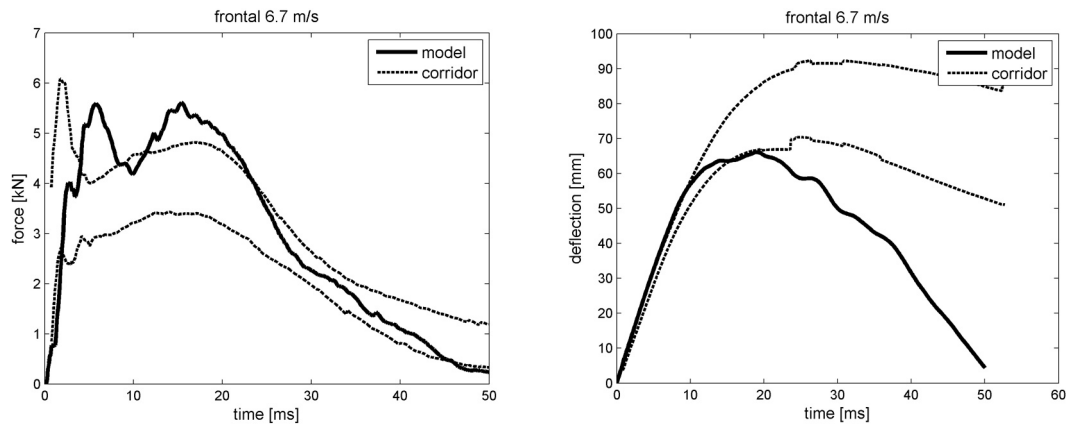


Fig. 5. The impactor contact force (left) and the thorax deflection (right) results of high speed frontal test

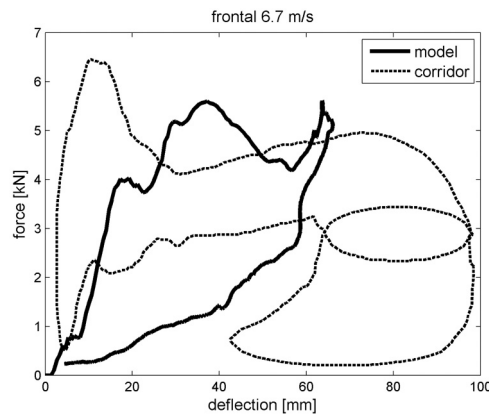


Fig. 6. The impactor contact force versus the thorax deflection for high speed frontal test

*Frontal impact — low speed (4.3 m/s)*

The contact impactor force results of the frontal test are shown in Fig. 7, left. The force fit the corridor for the first few milliseconds and then it increased above the corridor. There was a second force peak which did not fit in the corridor trend and range. The resulting thorax deflection (Fig. 7, right) fit the corridor until 15 ms and then it decreased below the corridor range. The contact impactor force versus thorax deflection results are shown in Fig. 8. Only the initial part fit the corridor. The occupant model thorax was stiffer compared to the experimental test.

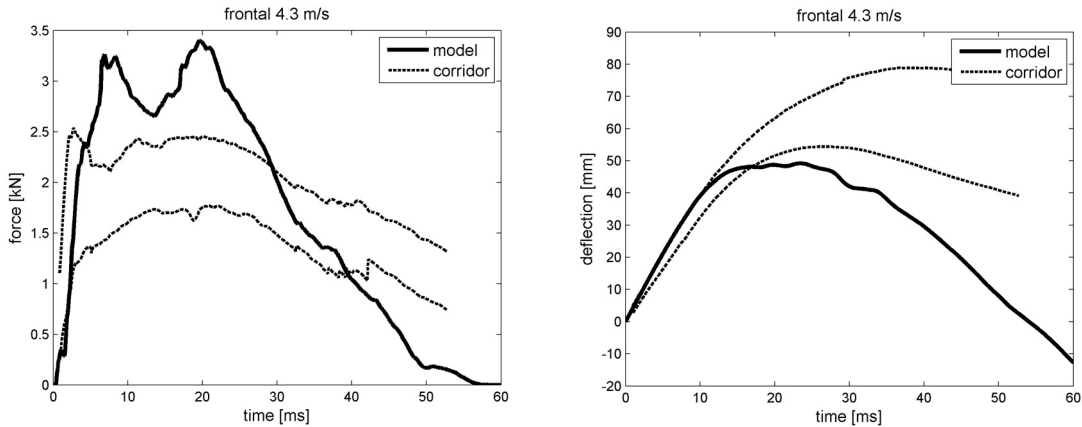


Fig. 7. The impactor contact force (left) and the thorax deflection (right) results of low speed frontal test

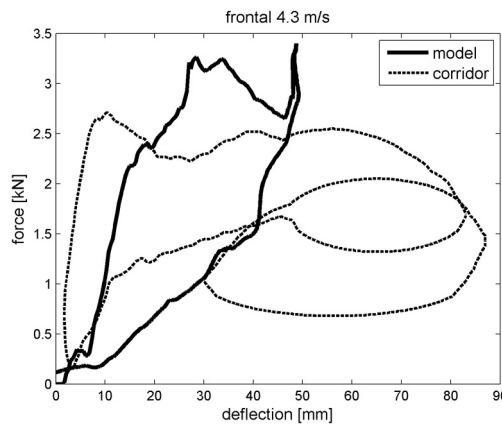


Fig. 8. The impactor contact force versus the thorax deflection for low speed frontal test

*Oblique impact — OSU*

The impactor contact force of the OSU oblique test is shown in Fig. 9, left. The simulation force response had a higher slope and its peak value was about 50 % higher than the corridor upper boundary. The thorax deflection (Fig. 9, right) was below the corridor range. The model response indicated that the model is too stiff in oblique impact scenario. The strain along the 5<sup>th</sup> ribs at the time of the highest deflection is shown in Fig. 10, right. There are negative strain values on the external side of the rib on the impacted side, positive strain values at the rear part of the rib on the impacted side, and lower strain values on the rib on the opposite side. The peak compressive strain on the right rib is around 80 % of the rib length, corresponding to strain profiles from the PMHS tests in oblique setup [10]. As well as for the frontal test, the thorax response was stiffer comparing to the experiment.

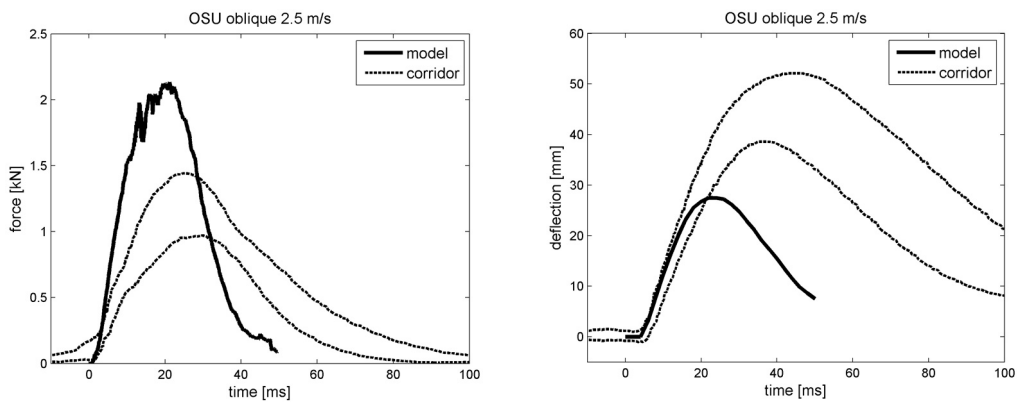


Fig. 9. The impactor contact force (left) and the thorax deflection (right) results of the oblique test

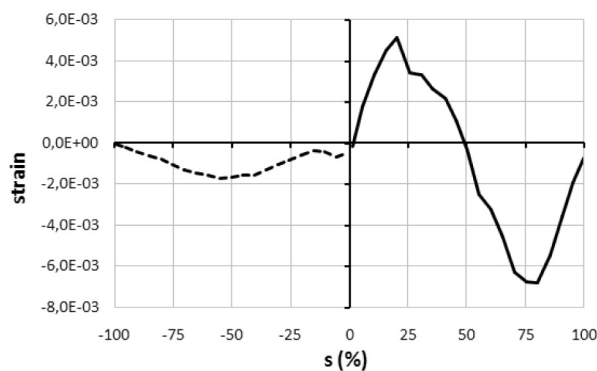


Fig. 10. Strain along the 5th ribs for the oblique test

### Lateral impact — OSU

The impactor contact force of OSU oblique test is shown in Fig. 11, left. The force had slower progress and its peak exceeded the upper corridor boundary slightly. The thorax deflection (Fig. 11, right) fit the corridor well almost to the end of the unloading phase. The strain along the 5th ribs at the time of the highest deflection is shown in Fig. 12, right. There are negative strain values on the external side of the rib on the impacted side, positive strain values at the rear part of the rib on the impacted side, and lower strain values on the rib on the opposite side. The peak strain on the right rib is around 65 % of the rib length, which is close to 60 % reported with the PMHS tests in lateral setup [10].

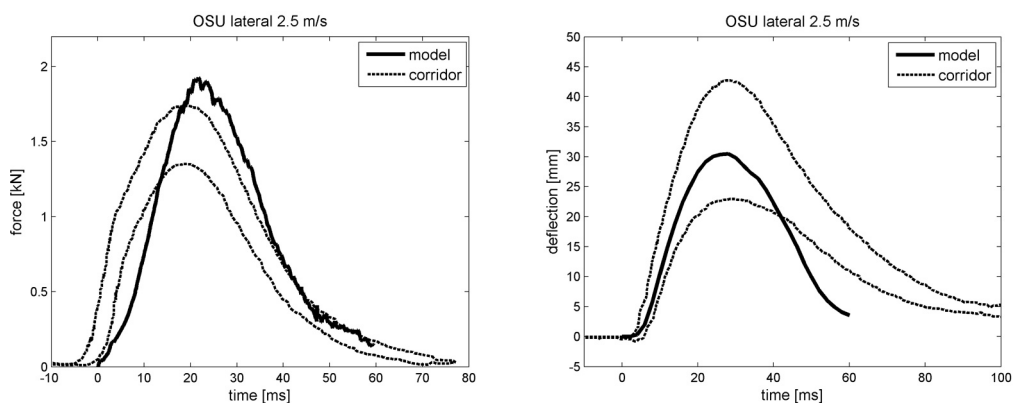


Fig. 11. The impactor contact force (left) and the thorax deflection (right) results of OSU lateral test

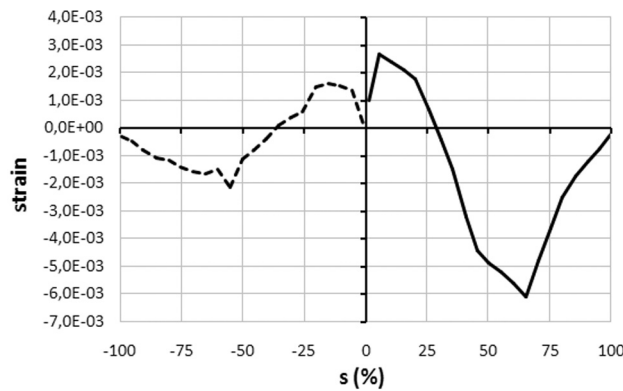


Fig. 12. Strain along the 5<sup>th</sup> ribs for the lateral test

### Lateral impact — HSRI

The contact impactor force results of the lateral test are shown in Fig. 13, left. The force fit the experimental corridor. The strain along the 5<sup>th</sup> ribs at the time of the highest deflection is shown in Fig. 13, right. There are negative strain values on the external side of the rib on the impacted side, positive strain values at the rear part of the rib on the impacted side, and lower strain values on the rib on the opposite side. The peak strain on the right rib is at same location as in OSU lateral setup, around 65 % of the rib length, which is close to 60 % reported with PMHS tests in lateral setup [10]. As well as for the OSU lateral impact, the model exhibits reasonable behaviour in the lateral impact.

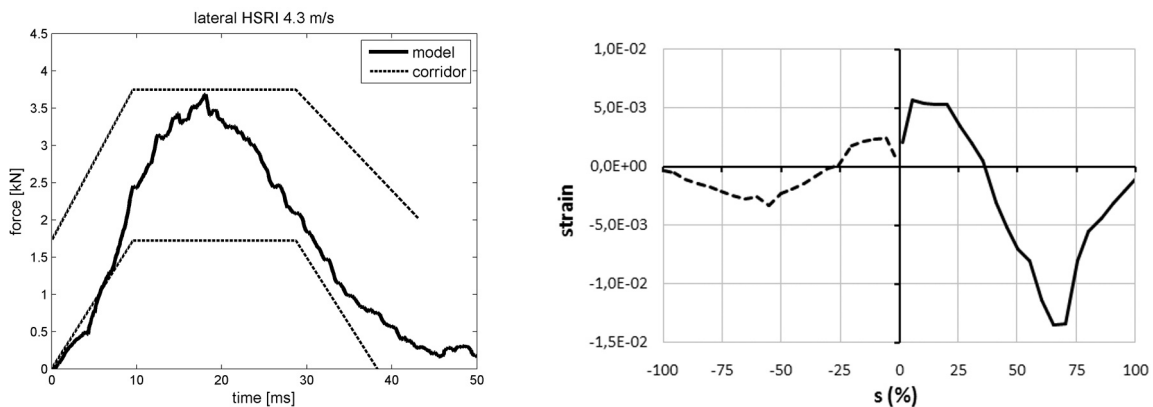


Fig. 13. The impactor contact force (left) and strain along the 5<sup>th</sup> ribs for HSRI lateral test

### 3.2. Influence of heart and lungs model on the global response

The frontal and oblique validation tests indicated that the model was stiffer than the PMHS during the experimental tests. In order to verify the influence of the thorax internal organs on the mechanical response of the model, the heart or lungs were removed from the model. Three tests were run with the altered model without heart — frontal low speed, OSU lateral and OSU oblique. In the frontal low speed test, the first peak of the contact impactor force decreased by 0.7 kN (Fig. 14, left) and the peak thorax deflection increased by 8 mm (Fig. 14, right) with respect to the reference model. There was no difference in the mechanical response of the OSU lateral and OSU oblique tests for this test configuration.

To assess the influence of the lungs on the mechanical response of the model, the left and the right lung were removed. Three tests were run with the altered model — frontal low speed, OSU lateral and OSU oblique. In the contact impactor force of frontal low speed test, there was

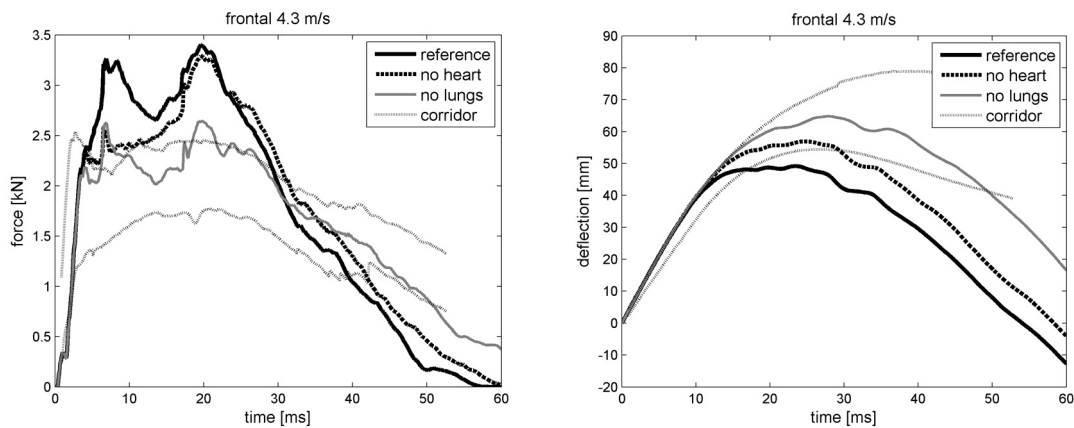


Fig. 14. The impactor contact force (left) and the thorax deflection (right) results of low speed frontal test of models with heart or lungs removed compared to the reference model

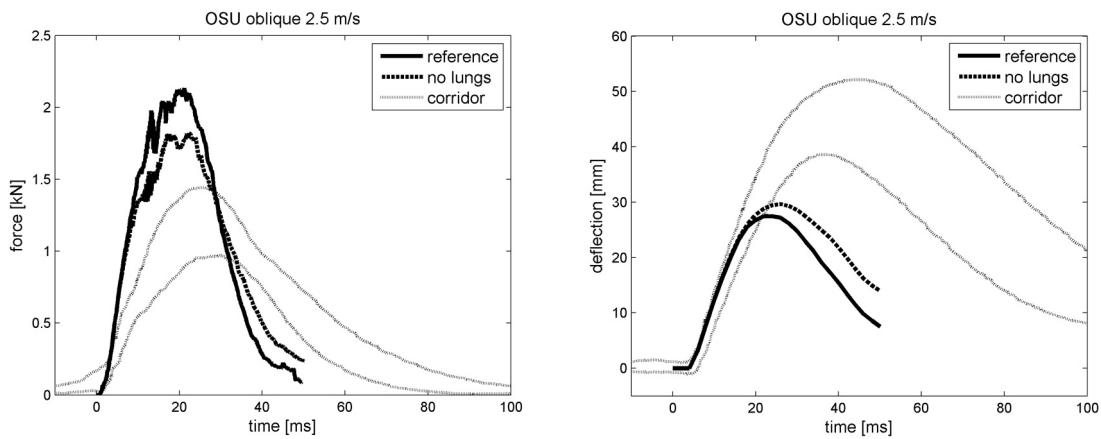


Fig. 15. The impactor contact force (left) and the thorax deflection (right) results of OSU oblique test of models with heart or lungs removed compared to the reference model

a significant decrease of 0.64 kN of the first peak and 0.75 kN of the second peak (Fig. 14, left) and the peak thorax deflection increased by 16 mm (Fig. 14, right).

There was no difference in the mechanical response of the OSU lateral test. In the OSU oblique test, the peak impactor contact force decreased by 0.32 kN (Fig. 15, left), the peak thorax deflection increased by 2 mm (Fig. 15, right).

The first peak of the impactor contact force and the thorax deflection in the frontal test were sensitive to the absence of the heart part. In the frontal test, the absence of the lungs significantly influenced both peaks of the contact impactor force and the thorax deflection. The lungs part also influenced the impactor contact force and thorax deflection in the OSU oblique test.

### 3.3. Influence of material parameters of heart and lungs on the global response

Modifications of the heart material slightly influenced the first peak of the impactor contact force (Fig. 16, left). The lowest value was found for Material 3, however this material model caused early termination of the simulation — at time 16.9 ms. Influence of the material choice on the second peak of the impactor force and the thorax deflection could be neglected (Fig. 16).

The simulations with most of the selected material models of lungs from Table 2 resulted with numerical instabilities and premature simulation termination. In terms of numerical stability, Material 7 was the best choice. The alteration of the lungs material model affected both the first

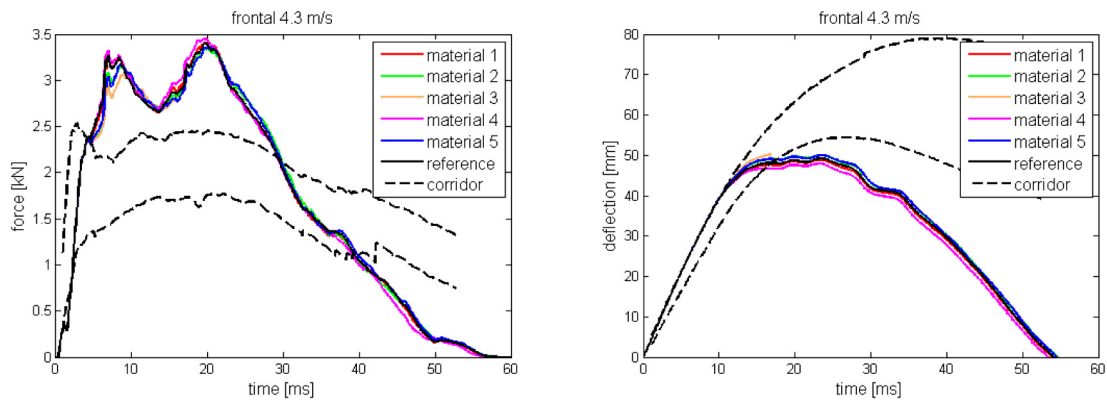


Fig. 16. The impactor contact force (left) and the thorax deflection (right) results of low speed frontal test with models with various material models of heart

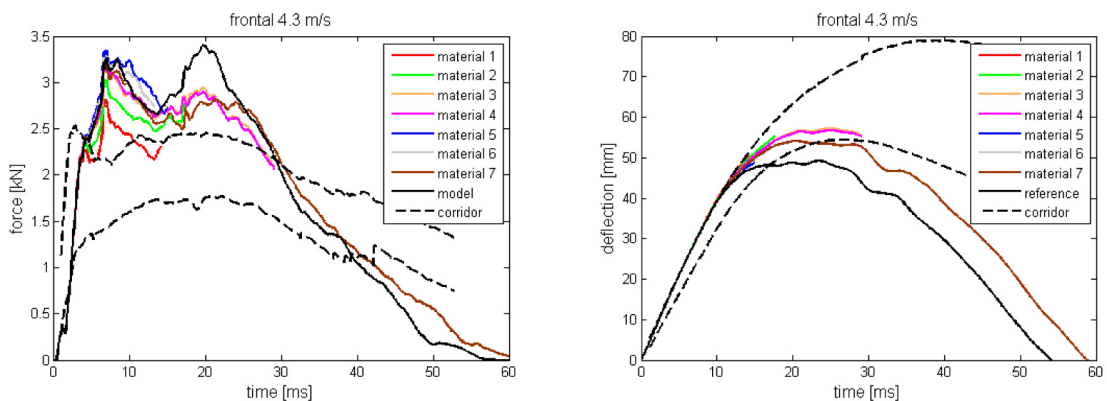


Fig. 17. The impactor contact force (left) and the thorax deflection (right) results of low speed frontal test with models with various material models of lungs

and the second peak of the impactor contact force, depending on the material choice (Fig. 17, left). The first peak was the lowest in case of Material 1. The second peak decreased for all material modifications. Thoracic deflection increased in all simulations (Fig. 17, right).

### 3.4. Influence of rib and sternum cortical bone material on the global response

For each model with altered Young’s modulus of the cortical bone, the first peak of the impactor force decreased and the thorax deflection slightly increased compared to the reference material model (Fig. 18). The most significant change was observed when both rib and sternum cortical bone material were altered at once (Fig. 18).

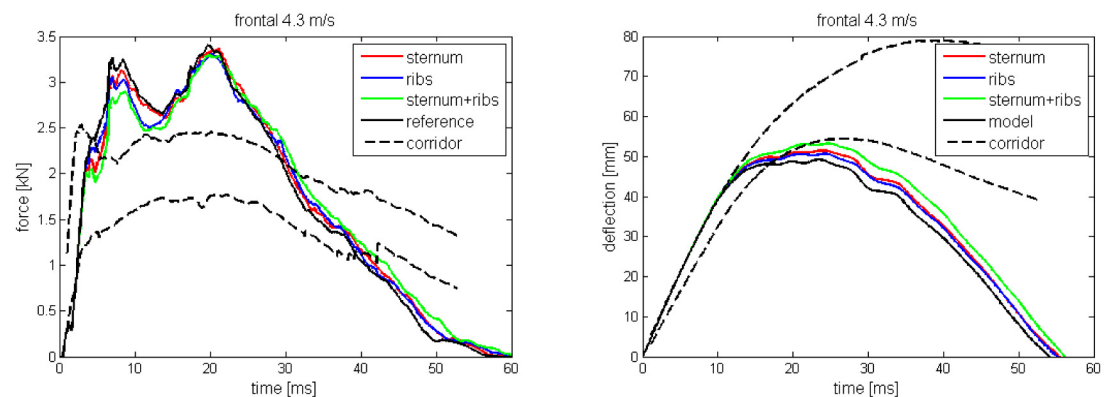


Fig. 18. The impactor contact force (left) and the thorax deflection (right) results of low speed frontal test with models with altered rib and sternum cortical bone material parameters

### 3.5. Influence of heart and lungs material combined with rib and sternum cortical bone material

As the next step, both rib and sternum cortical bone materials were altered. For the heart model, Material 2, 3 and 5 properties were chosen. For the lungs model, Material 4 and 7 were applied. The material models were adjusted based on the mechanical response that was the closest to the corridors. Although the simulation with lungs Material 4 ended with errors when lungs material properties only were altered, in combination with heart Material 2 and 5 the simulations ended normally (Fig. 20). The simulation with heart Material 3 and lungs Material 4 was unstable; however, combination of heart Material 3 with lungs Material 7 terminated normally (Fig. 19). The simulations with lungs Material 7 had the second peak of impactor contact force slightly lower and delayed by approximately 5 ms compared to the lungs Material 4 (Fig. 19, left). The deflection in the simulations with lungs Material 7 was slightly lower than the one in the simulations with lungs Material 4 (Fig. 19, right).

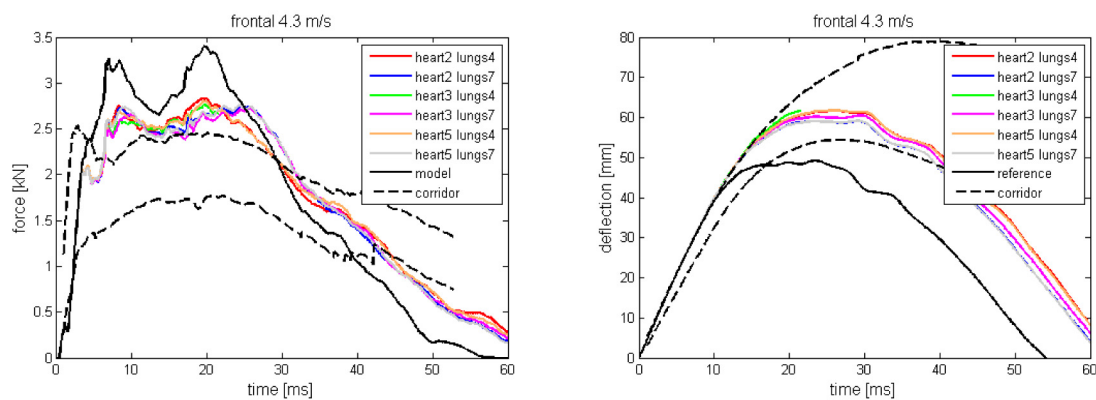


Fig. 19. The impactor contact force (left) and the thorax deflection (right) results of low speed frontal test with models with combination of altered heart and lungs material parameters

The parameter IHQ affecting the hourglassing was changed from a stiffness form of type 2 Flanagan-Belytschko (IHQ = 4) to Flanagan-Belytschko with exact volume integration (IHQ = 3) and tested in three material combinations in frontal scenario — first with combination of heart Material 2 and lungs Material 4, second with heart Material 5 and lungs Material 7 and third with heart Material 2 and lungs Material 7. These material combinations were selected because the simulations ended normally in the low speed frontal test (Fig. 19). No significant effect of the parameter IHQ variation on the model response was observed.

To verify the effect of heart and lungs material modifications on the global response in the oblique and lateral scenarios, three models were tested — first with combination of heart Material 2 and lungs Material 4, second with heart Material 5 and lungs Material 7 and third with heart Material 2 and lungs Material 7. These material combinations were selected because the simulations ended normally in the low speed frontal test (Fig. 19). All three models had altered rib and sternum cortical bone material (Table 3) because it provided model response closer to the corridors. As the results showed that the heart Material 2 and lungs Material 7 had almost no hourglassing effect, their combination was tested as well.

In the oblique scenario, the peak impactor contact force decreased by 7 % and the thorax deflection increased by 12 %, both getting closer to the corridors (Fig. 20). In lateral scenario, the peak impactor contact force decreased by 5 %, with the peak values getting almost into the corridors (Fig. 21, left). The thorax deflection increased approximately by 20 % and the unloading phase remained within the corridor for additional 11 ms of the simulation (Fig. 21, right).

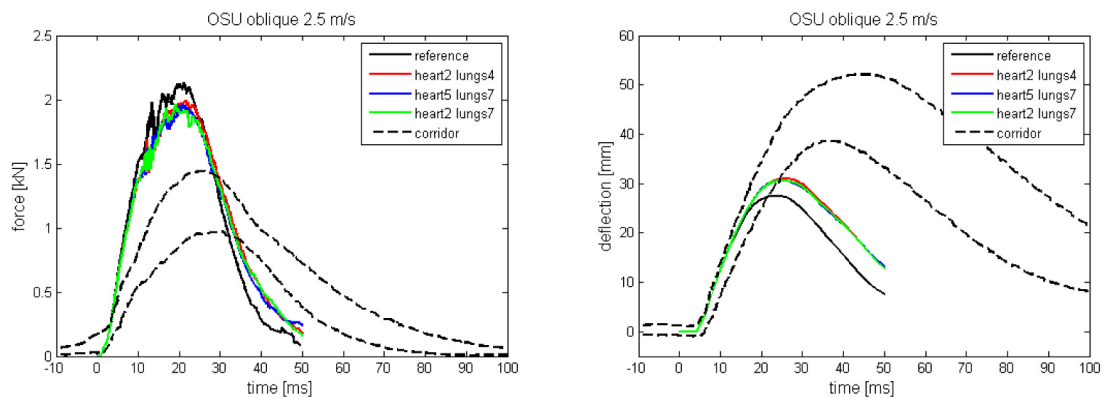


Fig. 20. The impactor contact force (left) and the thorax deflection (right) results of OSU oblique test with models with combination of altered heart and lungs material parameters

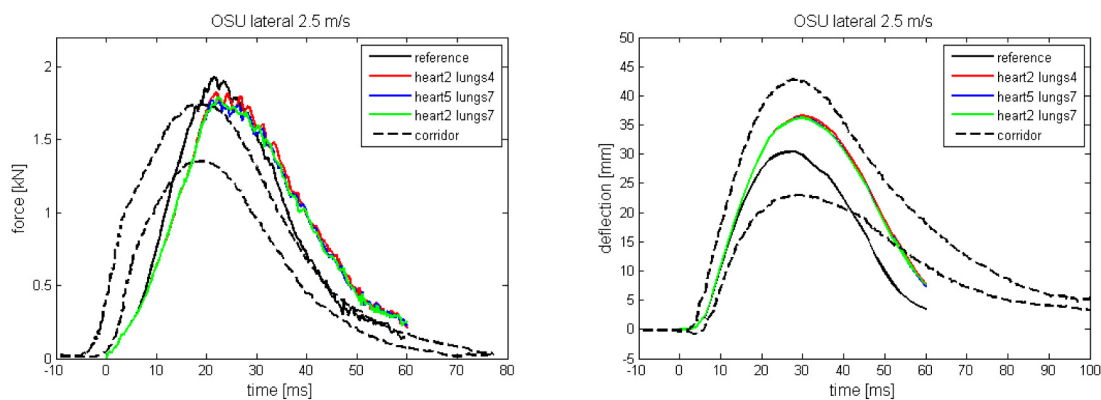


Fig. 21. The impactor contact force (left) and the thorax deflection (right) results of OSU lateral test with models with combination of altered heart and lungs material parameters

#### 4. Discussion

A series of pendulum impact simulations using the reference material models has been performed. The model response was tested in three impact scenarios: frontal, lateral and oblique.

The frontal impact with the high speed shows good performance in the model during the loading phase (Fig. 5). The force dependent on deflection copies the experimental response with just a small time shift. Although the unloading phase is faster, concerning the injury prediction, the global response is well validated taking into account the maximum values of force and deflection and the shape of curves. Fig. 6 is just a consequence of the combination of curves on Fig. 5.

The low speed frontal impact shows worse behaviour (Fig. 7). The problem might be caused by the higher overall stiffness of the model in order to fit the high speed response. Taking into account the potential injury predictability and good high speed response, the model is tuned to be used in safety applications.

The oblique impact shows higher stiffness and faster unloading phase. The problem is probably caused by the simplicity of the model, because in the biological reality, the human thorax is softer in the oblique direction. Taking into account the potential injury predictability, the model should be tuned for injury risk assessment also in the oblique impact.

The OSU lateral impact shows almost perfect behaviour of the model, where the signal obtained from the calculations fits the experimental signal corridor quite well. The same behaviour can be observed in the HSRI lateral impact, where the model response fits the corridor.

Additionally, the analysis concerning the model design was also performed. It focused on variation of material properties of the internal organs, which were assumed to constitute the differences between model behaviour and experimental reference, to verify the effect of material modifications on the global response and tune the model with the experimental corridors. The analysis shows significant improvement of the model response in frontal impact. It is caused mainly by different models of lungs and by altering rib and sternum parameters.

Taking the results into account, the model can be perfectly used for injury analysis in the lateral direction. The frontal and oblique impacts shows higher stiffness of the model, however, concerning the injury risk predictability the model is safe to be used for impact analysis.

## **5. Conclusion**

The parametric study and validation of the 50th percentile THOMO model were performed. The model response was tested in three impact scenarios: frontal, lateral and oblique.

In the frontal test scenarios, the initial mechanical response of the model was too stiff, compared to the reference experimental tests for high speed and low speed impact. For oblique test, the initial mechanical response was too stiff as well. For lateral tests, the results correspond reasonably to the corridors from PMHS tests.

The material properties of the major thoracic internal organs (heart and lungs) and the rib and sternum cortical bone were found to have a major influence on the thoracic response mainly in the frontal impact. Adjusting the material properties could improve the global response of the model.

Shift in the strain profile between lateral and oblique tests setup is around 15 %. The value of 20 % is observed in PMHS tests [10].

## **Acknowledgements**

This paper is a part of the THOMO project (<http://www.thomo.eu>) co-funded by the FP7 of the European Commission. The authors would like to gratefully thank the project partners, the GHBM and the COE. The contents of this publication are sole the responsibility of the authors and do not necessarily represent the views of the EC and of the GHBM.

## **Reference**

- [1] Brodin, K., Mendoza-Vazquez, M., Song, E., Lecuyer, E., Davidsson, J., Design implication for improving an anthropometric test device based on human body simulations, Proceedings of the International IRCOBI Conference, Dublin, Ireland, 2012, pp. 843–855.
- [2] Deng, Y. C., Kong, W., Ho, H., Development of a finite element human thorax model for impact injury studies, SAE International Congress and Exposition, Detroit, Michigan, SAE Paper 1999-01-0715, 1999.
- [3] GHBM website: <http://www.ghbmc.com>.
- [4] Gierczycka-Zbrożek, D., Rzymkowski, C., Toczyski, J., Influence of the material definition on the biomechanical response of a simplified human torso FE model, Proceedings of the 9<sup>th</sup> International Forum of Automotive Traffic Safety, Changsha, China, 2011, pp. 231–238.
- [5] Haug, E., Beaugonin, M., Montmayeur, N., Marca, C., Choi, H., Towards legal virtual crash tests for vehicle occupant safety design using human models, International Crashworthiness and Design Symposium, 2003.

- [6] Iwamoto, M., Nakahira, Y., Tamura, A., Kompars, H., Watanabe, I., Miki, K., Development of advanced human models in THUMS, Proceedings of the 6<sup>th</sup> European LS-DYNA Users' Conference, Gothenburg, Sweden, 2007, pp. 47–56.
- [7] Kimpara, H., Lee, J. B., Yang, K. H., King, A. I., Iwamoto, M., Watanabe, I., Miki, K., Development of a three-dimensional finite element chest model for the 5<sup>th</sup> percentile female, *Stapp Car Crash Journal* 49 (2005) 251–269.
- [8] Kroell, C., Schneider, D., Nahum, A., Impact tolerance and response of the human thorax, SAE Technical Paper 710851, 1971, doi:10.4271/710851.
- [9] Kroell, C., Schneider, D., Nahum, A., Impact tolerance and response of the human thorax II, SAE Technical Paper 741187, 1974, doi:10.4271/741187.
- [10] Leport, T., Baudrit, P., Potier, P., Trosseille, X., Lecuyer, E., Vallancien, G., Study of rib fracture mechanisms based on the rib strain profiles in side and forward oblique impact, *Stapp Car Crash Journal* 55 (2011) 99–250.
- [11] Lizee, E., Robin, S., Song, E., Bertholon, N., Le Coz, J.-Y., Besnault, B., Lavaste, F., Development of a 3D finite element model of the human body, SAE Technical Paper 983152, 1998, doi:10.4271/983152.
- [12] Robin, S., HUMOS: Human model for safety — A joint effort towards the development of refined human-like car occupant models, Proceedings of the 17<sup>th</sup> International Technical Conference on the Enhanced Safety of Vehicles, Paper No. 297, Amsterdam, 2001.
- [13] Robbins, D. H., Lehman, R. J., Nusholtz, G. S., Melvin, J. W., Benson, J. B., Stalnaker, R. L., Culver, R., Quantification of thoracic response and injury: the gathering of data; Final Report, Contract DOT-HS-4-00921, 1982.
- [14] Ruan, J., El-Jawahri, R., Chai, L., Barbat, S., Prasad, P., Prediction and analysis of human thoracic impact responses and injuries in cadaver impact using a full human body finite element model, *Stapp Car Crash Journal* 47 (2003) 299–321.
- [15] Shaw, J. M., Herriott, R. G., McFadden, J. D., Donnelly, B. R., Bolte, J. H., Oblique and lateral impact response of the PMHS thorax, *Stapp Car Crash Journal* 50 (2006) 147–167.
- [16] Shigeta, K., Kitagawa, Y., Yasuki, T., Development of next generation human FE model capable of organ injury prediction, Proceedings of the 21<sup>st</sup> International Technical Conference on the Enhanced Safety of Vehicles, Paper No. 09-0111, Stuttgart, 2009.
- [17] Vezin, P., Verriest, J., Development of a set of numerical human models for safety, Proceedings of the 19<sup>th</sup> International Technical Conference on the Enhanced Safety Vehicles Conference, Paper No. 05-0163, Washington D.C., 2005.
- [18] Wang, H.-C. K., Development of a side impact finite element thorax model, Ph.D. Thesis, Wayne State University, Detroit, 1995.
- [19] Yamada, H., *Strength of Biological Materials*, Williams & Wilkins Company, Baltimore, 1970.
- [20] Yang, K. H., Hu, J. W., White, N. A., King, A. I., Chou, C. C., Prasad, P., Development of numerical models for injury biomechanics research: A review of 50 years of publications in the Stapp Car Crash Conference, *Stapp Car Crash Journal* 50 (2006) 429–490.
- [21] Yoganandan, N., Pintar, F. A., Biomechanics of human thoracic ribs, *Journal of Biomechanical Engineering* 120 (1998) 100–104.
- [22] Yuen, K. F., The development of numerical human body model for the analysis of automotive side impact lung trauma, Master Thesis, University of Waterloo, Canada, 2009.
- [23] Zhao, J., Narwani, G., Development of a human body finite element model for restraint system R&D applications, Proceedings of the 19<sup>th</sup> International Technical Conference on the Enhanced Safety of Vehicles, Paper No. 05-0399, Washington D.C.; 2005.